

# Kondo-like behaviors in magnetic and thermal properties of single crystal $\text{Tm}_5\text{Si}_2\text{Ge}_2$

J. H. Kim<sup>1</sup>, S. J. Kim<sup>1</sup>, C. I. Lee<sup>1</sup>, M. A. Jung<sup>1</sup>, H. J. Oh<sup>1,2</sup>, Jong-Soo Rhyee<sup>3</sup>, Younghun Jo<sup>4</sup>, Hiroyuki Mitani<sup>5,6</sup>, Hidetoshi Miyazaki<sup>5</sup>, Shin-ichi Kimura<sup>5,7</sup>, and Y. S. Kwon<sup>1\*</sup>

<sup>1</sup> *Department of Physics, Sungkyunkwan University, Suwon 440-746, South Korea*

<sup>2</sup> *Department of Ophthalmic Optics, Masan College, Masan 630-729, Republic of Korea*

<sup>3</sup> *Inorganic Materials Group, Samsung Advanced Institute of Technology, Yong-In 446-712, Republic of Korea*

<sup>4</sup> *Nano Materials Research Team, Korea Basic Science Institute, Daejeon 305-333, Korea*

<sup>5</sup> *UVSOR Facility, Institute for Molecular Science, Okazaki 444-8585, Japan*

<sup>6</sup> *Graduate School of Engineering, Shinshu University, Nagano 380-8553, Japan*

<sup>7</sup> *School of Physical Sciences, The Graduate University for Advanced Studies (SOKENDAI), Okazaki 444-8585, Japan*

(Dated: November 2, 2018)

We grew the single crystal of stoichiometric  $\text{Tm}_5\text{Si}_{2.0\pm 0.1}\text{Ge}_{2.0\pm 0.1}$  using a Bridgeman method and performed XRD, EDS, magnetization, ac and dc magnetic susceptibilities, specific heat, electrical resistivity and XPS experiments. It crystallizes in orthorhombic  $\text{Sm}_5\text{Ge}_4$ -type structure. The mean valence of Tm ions in  $\text{Tm}_5\text{Si}_{2.0\pm 0.1}\text{Ge}_{2.0\pm 0.1}$  is almost trivalent. The 4f states is split by the crystalline electric field. The ground state exhibits the long range antiferromagnetic order with the ferromagnetically coupled magnetic moments in the *ac* plane below 8.01 K, while the excited states exhibit the reduction of magnetic moment and magnetic entropy and  $-\log T$ -behaviors observed in Kondo materials.

PACS numbers: 72.15.Qm, 75.20.Hr, 65.40.Ba

## I. INTRODUCTION

Interest in  $\text{R}_5(\text{Si}_x\text{Ge}_{1-x})_4$  pseudobinary compounds (R=rare-earth metals) has been revived with the recent discovery by Pecharsky and Gschneidner [1, 2] of a giant magnetocaloric effect (MCE) in  $\text{Gd}_5(\text{Si}_x\text{Ge}_{1-x})_4$ . This effect has potential applications in magnetic refrigerants. The giant MCE in  $\text{Gd}_5(\text{Si}_x\text{Ge}_{1-x})_4$  is caused by the first-order magnetic transition that accompanies a martensitic-like structure phase transition [3, 4]. In  $\text{Gd}_5(\text{Si}_x\text{Ge}_{1-x})_4$ , strong coupling between the magnetic and crystallographic lattices is also responsible for the giant magnetoresistance and strong magnetoelastic effect [3, 5]. In order to understand the physical mechanism for the interesting behaviors observed in the  $\text{R}_5(\text{Si}_x\text{Ge}_{1-x})_4$  family of intermetallic compounds, it is important to examine their magnetic and crystallographic structures. The magnetic structure of  $\text{Gd}_5\text{Si}_2\text{Ge}_2$  was determined by x-ray resonant magnetic scattering experiments [6]. However, the magnetic structure of  $\text{Gd}_5(\text{Si}_x\text{Ge}_{1-x})_4$  has not been determined because of the huge neutron absorption cross section of the Gd isotope. Therefore, the magnetic and thermal properties of many binary and pseudobinary compounds of the form  $\text{R}_5(\text{Si}_x\text{Ge}_{1-x})_4$ , with rare-earth (R) ions excepting Gd ion are being re-examined [7, 8, 9, 10, 11, 12, 13, 14].

$\text{Tb}_5(\text{Si}_x\text{Ge}_{1-x})_4$  compounds also exhibit a giant magnetocaloric effect around  $x=0.5$  [15]. Initially, this phenomenon was understood to be the result of strong coupling of the magnetic and crystallographic sublattices as in  $\text{Gd}_5(\text{Si}_x\text{Ge}_{1-x})_4$  near  $x=0.5$  [9]. However, no

clear metamagnetic-like behavior, such as that found in  $\text{Gd}_5\text{Si}_2\text{Ge}_2$  was observed in the magnetization of polycrystalline  $\text{Tb}_5\text{Si}_2\text{Ge}_2$ . A neutron powder diffraction study of this compound revealed decoupling of the structural and magnetic transitions with a separation of 10 K [10]. It was also revealed that, upon cooling, long-range ferromagnetism exists in the monoclinic  $P112_1/a$  structure before its structural transformation into orthorhombic  $Pnma$ .

On the other hand,  $\text{Yb}_5(\text{Si}_x\text{Ge}_{1-x})_4$  alloys preserve the same crystal structure as  $x$  varies from 0 to 4 [18]. Therefore, the replacement of Ge with Si and vice versa has little effect on the magnetic properties of these materials, which were thought to be a unique feature compared to the other  $\text{R}_5\text{T}_4$  systems. Three different lattice sites accommodating lanthanides in the  $\text{Gd}_5\text{Si}_4$ -type crystal structure exhibit selectivity with respect to the valence states of Yb ions. Nonmagnetic  $\text{Yb}^{2+}$  ions are located in the 4c sites and one of the 8d sites, whereas  $\text{Yb}^{3+}$  ions are located exclusively in the 8d sites [18].  $\text{Yb}_5(\text{Si}_x\text{Ge}_{1-x})_4$  may be a heterogeneous mixed valence system. All  $\text{Yb}_5(\text{Si}_x\text{Ge}_{1-x})_4$  alloys show weak antiferromagnetic correlations at temperatures between 2.4 K and 3.2 K [18].

$\text{R}_5(\text{Si}_x\text{Ge}_{1-x})_4$  systems with heavy lanthanides other than Gd, Tb, and Yb (mentioned above) have been studied to some extent. Recently, phase diagrams of the pseudobinary systems with R=Er [12, 19] and Y [21] have been constructed. Selected  $\text{R}_5(\text{Si}_x\text{Ge}_{1-x})_4$  compounds for R=La [22, 23], Ce [30], Pr [8, 24, 25], Nd [7, 11, 26], Sm [31], Dy [28], and Lu [29] have also been reported about their crystalline structures, magnetisms and magnetic caloric effects. Especially, although the Kondo effect is expected to be observed in the compounds with R=Ce [30] Yb [18] and Sm [31], there are no reports on the Kondo effect.

\*Electronic address: yskwon@skku.ac.kr

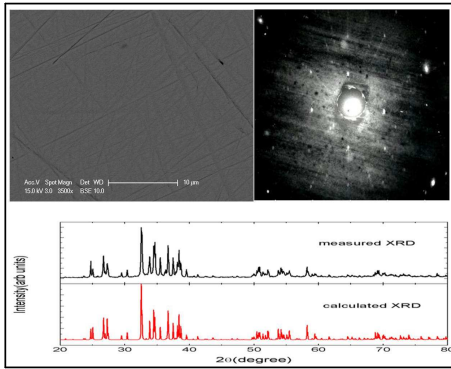


FIG. 1: (color online). (a) Scanning electron microscopy (SEM) image of the polished surface of  $\text{Tm}_5\text{Si}_2\text{Ge}_2$  single crystal. (b) Laue diffraction pattern image in the  $ac$ -plane of a  $\text{Tm}_5\text{Si}_2\text{Ge}_2$  single crystal. (c) The measured and calculated x-ray diffraction patterns of a  $\text{Tm}_5\text{Si}_2\text{Ge}_2$  single crystal.

In case of  $R=\text{Tm}$  only the crystallographic data for the  $\text{Tm}_5\text{T}_4$  binary compounds ( $T=\text{Si}$  or  $\text{Ge}$ ) have been reported [32], but their physical properties have not been examined. In addition, since the  $\text{Tm}$  can have valences of +2 or +3, the magnetic ordering, the valence fluctuation or the Kondo effect might be observed such as  $\text{TmX}$  ( $X$ : chalcogen) and thus this study on  $\text{Tm}_5\text{Si}_2\text{Ge}_2$  is very important.

## II. EXPERIMENTAL DETAILS

A single crystal of  $\text{Tm}_5\text{Si}_2\text{Ge}_2$  was grown using the Bridgeman method at  $1950^\circ\text{C}$  in a pure tungsten crucible that had been previously baked out at  $2200^\circ\text{C}$ . The tungsten crucible never reacts with the constitutive elements. Because of the high volatility of  $\text{Tm}$ , the starting materials were sealed in welded tungsten crucible using an electron beam welder. Some  $\text{Tm}$  evaporates and might settle somewhere else in the crucible. Therefore  $\text{Tm}$ ,  $\text{Si}$ , and  $\text{Ge}$  at a ratio of  $5.02 : 2 : 2$  were used as starting materials. The crystal had a diameter of 10 mm and a length of 12 mm, and was well cleaved along the  $ac$  crystallographic plane.  $\text{Tm}$  metal was obtained from a commercial vendor and was 99.9 at.% pure with the following major impurities (in at.%):  $\text{Fe}$ -0.01,  $\text{Ca}$ -0.03,  $\text{Mg}$ -0.01,  $\text{Ni}$ -0.01,  $\text{Al}$ -0.01,  $\text{T}$ -0.01,  $\text{Si}$ -0.01,  $\text{C}$ -0.015,  $\text{O}$ -0.05, and  $\text{Cl}$ -0.05. The elements  $\text{Si}$  and  $\text{Ge}$  were also purchased from a commercial vendor, and were better than 99.999 at.% purity. The orientation of the  $b$  crystallographic axis and  $ac$  plane in the sample were established using the backscattered Laue method.

The magnetic measurements were performed using a SQUID magnetometer (MPMS XL, Quantum Design). The magnetic susceptibility of the zero-magnetic-field cooled and magnetic-field cooled samples was measured

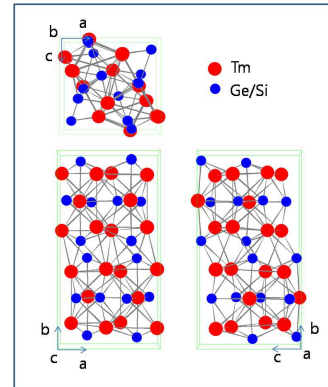


FIG. 2: (color online). Orthorhombic  $\text{Sm}_5\text{Ge}_4$ -type crystal structure with space group  $Pnma$

as a function of temperature from 2 to 300 K at  $H=100$  Oe. Isothermal magnetization was measured at 2, 4, and 6 K in a DC magnetic field varying from 0 to 5 T for the zero-magnetic-field cooled and magnetic-field cooled samples. The specific heats of  $\text{Tm}_5\text{Si}_2\text{Ge}_2$  and  $\text{Lu}_5\text{Si}_2\text{Ge}_2$  were measured using a physical property measurement system (PPMS, Quantum Design). The former was measured in various magnetic fields, ranging from 0 to 9 T, and oriented parallel to the  $b$  crystallographic axis.

The mean valence of  $\text{Tm}$ -ions in  $\text{Tm}_5\text{Si}_2\text{Ge}_2$  was examined by X-ray photoemission spectroscopy (XPS,  $\text{Mg } K\alpha$  line,  $h\nu=1253.6$  eV) of the  $\text{Tm } 4d$  and  $4p$  core levels using a 100-mm radius hemispherical photoelectron analyzer (VG Scienta SES-100). The base pressure of the chamber was less than  $2 \times 10^{-8}$  Pa. The sample temperature and total energy resolution were set to approximately 20 K and 0.7 eV, respectively. To obtain the mean valence of  $\text{Tm}_5\text{Si}_2\text{Ge}_2$ , the  $\text{Tm } 4d$  and  $4p$  core level XPS spectra of  $\text{TmS}$  (mostly  $\text{Tm}^{3+}$ ) and  $\text{TmTe}$  (mostly  $\text{Tm}^{2+}$ ) were also measured for the reference. [43] Clean sample surfaces were prepared inside the ultra high vacuum chamber by scraping with a clean diamond filler. After cleaning, the level of oxygen and carbon contaminations was checked by monitoring the intensity of the  $\text{O } 1s$  and  $\text{C } 1s$  photoemission peaks. The intensities of the  $\text{O } 1s$  and  $\text{C } 1s$  peaks were kept within the noise level during the measurements.

## III. EXPERIMENTAL RESULTS AND DISCUSSION

As shown in Fig. 1(a), atomic number sensitive back-scattered electron (BSE) imaging of the polished surface of single crystal  $\text{Tm}_5\text{Si}_2\text{Ge}_2$  showed that the sample contained a single phase, which was identified as  $\text{Tm}_5\text{Si}_{2.0\pm 0.1}\text{Ge}_{2.0\pm 0.1}$  by EDS (Energy Dispersive Spectroscopy). Fig. 1(b) shows the imaging of the pattern

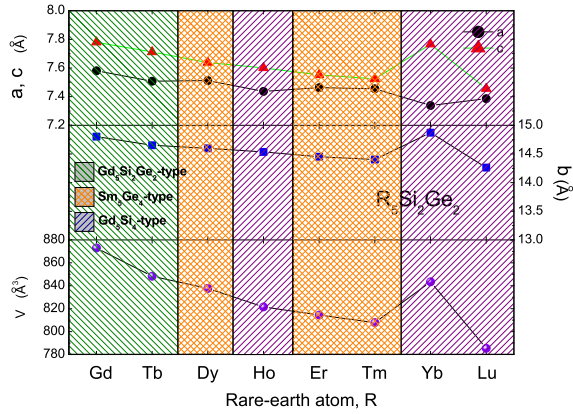


FIG. 3: (color online). Variation of the lattice parameters of  $R_5Si_2Ge_2$  with  $R=Gd$  through to  $Lu$

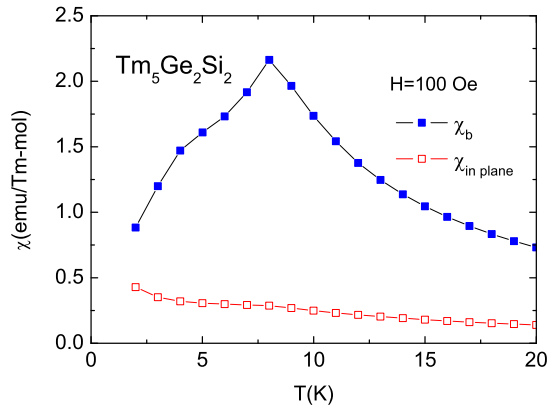


FIG. 4: (color online). Temperature dependence of the magnetic susceptibility of a  $Tm_5Si_2Ge_2$  single crystal for the  $H||b$ -axis and  $H||ac$ -plane in low temperature regions.

of Laue diffraction for single crystal  $Tm_5Si_2Ge_2$ . The Laue pattern was formed the x-rays diffracted from the  $ac$ -plane of  $Tm_5Si_2Ge_2$ . Fig. 1(c) shows the x-ray diffraction pattern of  $Tm_5Si_2Ge_2$ . The peaks positions in the pattern are consistent with the diffraction pattern calculated from an orthorhombic  $Sm_5Ge_4$ -type crystal structure (space group  $Pnma$ ), which is plotted in Fig. 2, with lattice constants  $a=7.455\pm 0.001$ ,  $b=14.402\pm 0.002$ , and  $c=7.525\pm 0.001$  Å.

Fig. 3 shows the change in the lattice parameters of  $R_5Si_2Ge_2$  with  $R=Gd$  through to  $Lu$ .  $R_5Si_2Ge_2$  is classified into three types of crystal structures, which makes it difficult to deduce the mixed valence of  $Tm_5Si_2Ge_2$ . It was possible to estimate the valence of  $R$ -ions because the three types of crystal structures are quite similar and contain four formula units in a unit cell. In  $R=Gd$  to  $Er$  and  $Lu$ , which are trivalent, the lattice parameters and volume of a  $R_5Si_2Ge_2$  unit cell decrease smoothly

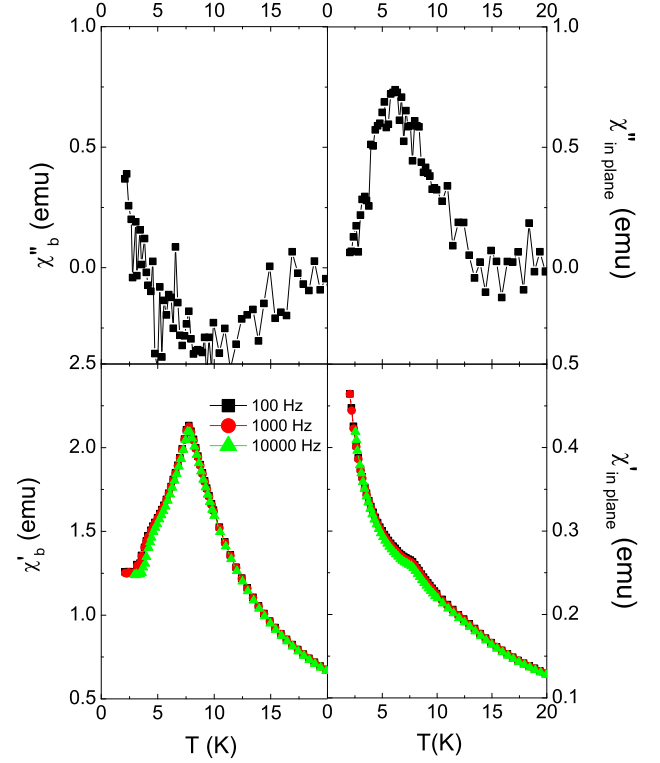


FIG. 5: (color online). Ac magnetic susceptibilities as a function of temperature for different frequencies in  $Tm_5Si_2Ge_2$  single crystal.

with increasing atomic number due to lanthanide contraction. In the case of  $R=Tm$ , the lattice parameters and unit cell volume were on the line indicating that  $Tm$  ion is trivalent. This result is inconsistent with those of the magnetic susceptibility and magnetization mentioned below. Note that the unit cell volume for  $R=Yb$  is smaller than that indicated from the line formed by the trivalent  $R$  ion, which means that  $Yb$  ions have an intermediate valence, as reported elsewhere.

Fig. 4 shows the temperature dependence of the magnetic susceptibility  $\chi$  of a single crystal of  $Tm_5Si_2Ge_2$  in the low temperature region. The magnetic susceptibilities were measured upon heating at  $H=100$  Oe with a magnetic field aligned parallel to the  $b$  crystallographic axis and the  $ac$  plane, i.e.  $\chi_b$  and  $\chi_{in-plane}$ , respectively. The magnetic susceptibilities of the zero-magnetic-field cooled and field cooled samples were the same.  $\chi_b$  shows a distinct peak at 8.0 K, which is due to antiferromagnetic ordering. Below  $T_N$ ,  $\chi_b$  approached zero, and then showed a shoulder at approximately 5 K. On the other hand, the  $\chi_{in-plane}$  below  $T_N$  was a constant down to approximately 5 K, and then increased with decreasing

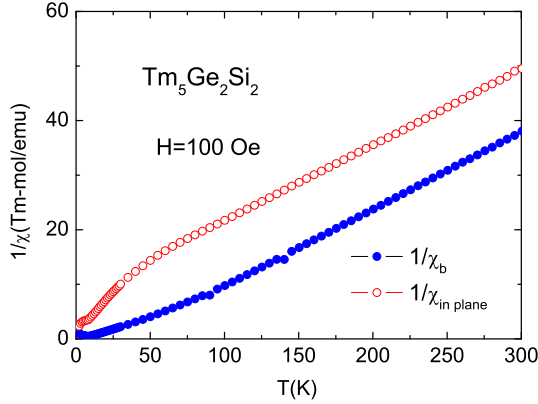


FIG. 6: (color online). Temperature dependence of the inverse magnetic susceptibility of a  $\text{Tm}_5\text{Si}_2\text{Ge}_2$  single crystal for the  $H\parallel b$ -axis and  $H\parallel ac$ -plane.

temperature. The behaviors of the magnetic susceptibility approaching zero in  $\chi_b$  and being constant in the  $\chi_{in-plane}$  immediately below  $T_N$  are also found in the conventional antiferromagnetic single crystals. This indicates that the magnetic moments of  $\text{Tm}_5\text{Si}_2\text{Ge}_2$  below  $T_N$  are coupled antiferromagnetically along the  $b$ -axis. The shoulder in the  $\chi_b$  and the increase in the  $\chi_{in-plane}$  at approximately 5 K were due to the magnetic moment coupled ferromagnetically in the plane, which will be discussed in the section reporting the ac magnetic susceptibility. Such antiferromagnetism was proposed by Landau for layered antiferromagnetic materials in which the magnetic moments in ferromagnetically-ordered layers alternate from layer to layer [34]. In  $\text{Gd}_5\text{Ge}_4$  the antiferromagnetism proposed by Landau was also observed at  $T_N=128$  K, and the strength of the exchange interactions for antiferromagnetism and ferromagnetism were equal [35]. However, there was anisotropy in the strength of the exchange interactions in  $\text{Tm}_5\text{Si}_2\text{Ge}_2$ .

To prove our claim regarding the layered magnetic orderings observed in  $\text{Tm}_5\text{Si}_2\text{Ge}_2$  the ac magnetic susceptibilities were measured as a function of temperature at different frequencies (Fig. 5). In  $\chi_b'$ , a peak was observed at 8 K and a bulge was observed at approximately 5 K, which is similar to the dc magnetic susceptibility. No frequency-dependence was found in the anomalies formed by the magnetic ordering, which suggests that the anomalies are caused by long range magnetic orderings.  $\chi_b''$  is independent of temperature below  $T_N$ , which suggests that magnetic ordering is not ferromagnetic. On the other hand, the  $\chi_{in-plane}'$  below  $T_N$  is constant down to approximately 5 K, and then increases with decreasing temperature, which is similar to the dc magnetic susceptibility. The  $\chi_{in-plane}''$  shows a peak at approximately 5 K, which is different from the feature in  $\chi_b'$ . The peak originates from a long range ferromagnetic ordering in the plane below 5 K because the peak in the imaginary

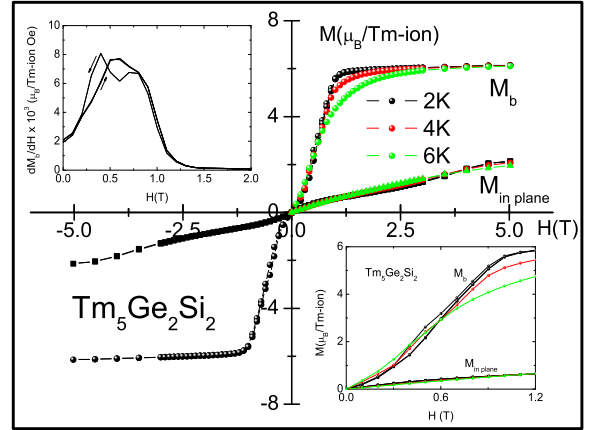


FIG. 7: (color online). Magnetic field dependence of the magnetization of a  $\text{Tm}_5\text{Si}_2\text{Ge}_2$  single crystal for the  $H\parallel b$ -axis and  $H\parallel ac$ -plane,  $M_b$  and  $M_{in-plane}$ , respectively, at  $T=2, 4$ , and  $6$  K. The inset plotted below shows  $M_b$  and  $M_{in-plane}$  in low magnetic fields, and the inset plotted above shows the derivatives of  $M_b$  with respect to the magnetic field at  $T=2$  K.

part of the magnetic susceptibility is formed by energy losses due to the hysteresis observed in ferromagnetic ordering. This strongly supports the claim for the magnetic ordering mentioned above.

Fig. 6 shows the temperature dependence of the inverse magnetic susceptibility  $1/\chi$ .  $1/\chi$  is linearly proportional to the temperature at temperature regions higher than 150K, and reflects the Curie-Weiss behavior with the paramagnetic Curie temperatures  $\Theta_{p,b}\sim 34$  K and  $\Theta_{p,in-plane}\sim 55$  K in the  $b$ -axis and the plane, respectively. The effective magnetic moment,  $p_{eff}$ , is equal to  $6.8 \pm 0.15 \mu_B/\text{Tm}$  atom in both directions. The anisotropy of  $\Theta_p$  may be due to the anisotropy of the exchange interactions or the crystalline electrical effect. The experimentally determined  $p_{eff}$  was between that of  $\text{Tm}^{3+}$  ( $p_{eff1}=7.57 \mu_B$ ) and  $\text{Tm}^{2+}$  ( $p_{eff2}=4.54 \mu_B$ ), which were determined theoretically calculated.

The isothermal magnetization of single crystal  $\text{Tm}_5\text{Si}_2\text{Ge}_2$  were measured at  $T=2, 4$ , and  $6$  K, as shown in Fig. 7, when a magnetic field was applied in the directions parallel to the  $b$  crystallographic axis and  $ac$  plane. The magnetization of the  $H\parallel b$  axis,  $M_b$ , was much larger than that of the  $H\parallel ac$  plane,  $M_{in-plane}$ , in the measured magnetic field regions, which suggests that the  $b$  axis is the easy axis. A metamagnetic transition below  $T_N$  was observed at  $H_{cr}=0.5$  T, as shown in the inset plotted in the bottom of Fig. 7. This is better seen as the peak in another inset, which shows the derivatives of the magnetization with respect to the magnetic field. The metamagnetic transition was attributed to a magnetic field induced spin-flip transformation. Remanence-free hysteresis was observed only at  $T=2$  K. As shown in the bottom inset,  $M_b$  increases with increasing temperature below

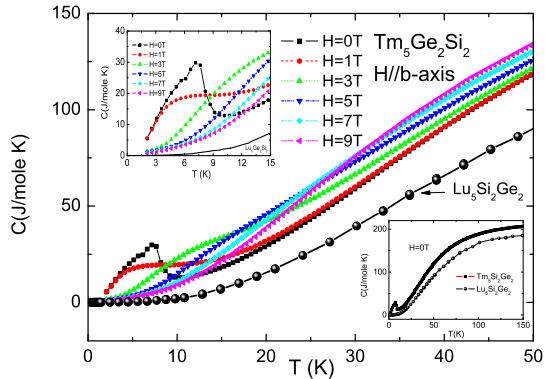


FIG. 8: (color online). Temperature dependence of the specific heats,  $C$ , of a  $\text{Tm}_5\text{Si}_2\text{Ge}_2$  single crystal in various magnetic fields for the  $H\parallel b$ -axis and  $\text{Lu}_5\text{Si}_2\text{Ge}_2$ . The left inset shows the specific heat in low temperature regions and the right inset shows the specific heat in measured temperature regions.

$H_{cr}$ . Hysteresis is generally observed in magnetic materials with narrow domain walls [36, 37, 38, 39]. In these magnetic materials, the motion of the walls is hindered by pinning centers at low temperatures, giving rise to small magnetization. As the temperature increases, thermal energy provides the driving force necessary to overcome the barriers created by the pinning centers, leading to an increase in magnetization with increasing temperature. The  $M_b$  remains below  $6.1 \pm 0.1 \mu_B$  per Tm-ion in a magnetic field of 5 T. The theoretically saturated magnetic moments of  $\text{Tm}^{3+}$  and  $\text{Tm}^{2+}$  are given by  $gJ=7 \mu_B$ ,  $M_{3+}$ , and  $gJ=4 \mu_B$ ,  $M_{2+}$ , respectively, where  $g$  is the gyromagnetic ratio and  $J$  is the total angular momentum quantum number. An intermediate magnetization value was also observed in the magnetically ordered state.  $M_{in-plane}$  in the  $ac$  plane increases slowly with increasing magnetic field with no distinct change at  $H_{cr}$ . This indicates that the metamagnetic transition is due to a flip of the magnetic moments in the  $ac$  plane.

The specific heat of the single crystal of  $\text{Tm}_5\text{Si}_2\text{Ge}_2$  was measured upon heating in various magnetic fields ranging from 0 to 9 T, which is shown in Fig. 8. The magnetic field was applied parallel to the  $b$  crystallographic axis. The antiferromagnetic transition which was observed at  $T_N=8.0$  K in the magnetic susceptibility measurements taken at  $H=100$  Oe is indicated by a sharp peak at 7.7 K in the specific heat measurements at  $H=0$  T. The mid-point temperature (8 K) of the peak in the specific heat curve is equal to  $T_N$ . When  $H>1$  T, the sharp peak becomes a broad shoulder and shifts to high temperature with further increasing in  $H$ . To demonstrate this feature distinctly, the phonon part in the specific heat of  $\text{Tm}_5\text{Si}_2\text{Ge}_2$  was excluded using the specific heat of the nonmagnetic  $\text{Lu}_5\text{Si}_2\text{Ge}_2$ . Fig. 9 shows the magnetic contribution to the specific heat. In the figure,

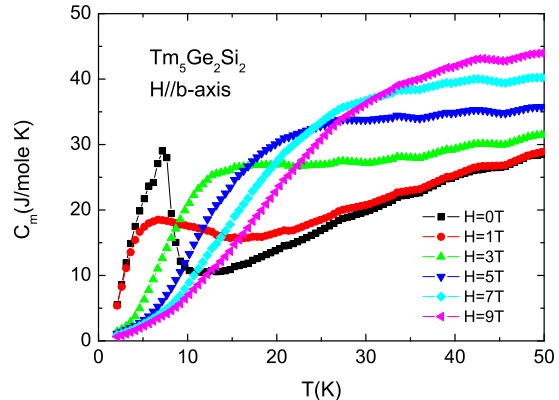


FIG. 9: (color online). Temperature dependence of the magnetic contribution ( $C_m$ ) to specific heats of  $\text{Tm}_5\text{Si}_2\text{Ge}_2$  single crystal in various magnetic fields for the  $H\parallel b$ -axis.

there appears to several small humps at approximately  $T=26, 33, 42$  K etc. These humps are due to errors occurring when subtracting the specific heat of  $\text{Lu}_5\text{Si}_2\text{Ge}_2$ , which were measured at rough temperature intervals. A shoulder was observed at approximately 7 K at  $H=1$  T, 12 K at  $H=3$  T, 18 K at  $H=5$  T, 28 K at  $H=7$  T, and 35 K at  $H=9$  T. The shoulder was formed by a Schottky anomaly due to excitation between the crystal-field splitting states, which are divided by the Zeeman effect under internal magnetic fields induced in ferromagnetism as well as in an applied magnetic field [40, 41, 42]. A weak anomaly was observed at 5.6 K in the specific heat curve at  $H=0$  T, as shown in the inset of Fig. 8. This was attributed to the ferromagnetic ordering in the plane observed in the magnetic susceptibility. This anomaly was not observed in  $H>1$  T because  $\text{Tm}_5\text{Si}_2\text{Ge}_2$  exhibits ferromagnetism. Fig. 10 shows the magnetic entropy per Tm mole evaluated from the integral of the magnetic contribution to the specific heat divided by temperature. The magnetic entropy at  $H=0$  T was nearly recovered to  $R\ln 2$  at  $T_N$ . This suggests that the ground state is a doublet considering the low symmetry of its crystal structure. In the high temperature regions, the magnetic entropy was saturated to approximately  $17.5 \text{ J/Tm-molK}^2$ , which is smaller than the full entropy for  $\text{Tm}^{3+}$  ions,  $R\ln 13$ . This is due to the reduced magnetic moment observed in the magnetic susceptibility and magnetization. The magnetic entropy in  $H>0$  T approaches the value at  $H=0$  T in the high temperature regions. The entropy decreases with increasing magnetic field across all temperatures, because of the Zeeman effect mentioned above.

However, it is unclear why the magnetic moment is reduced. Decreases in the magnetic moments of Tm ions might arise from the mixed valent state, spin frustration, Kondo effect etc. Assuming that there are two distinct Tm valence states in the lattice, the fraction of each ion can be estimated from the experimentally evaluated ef-

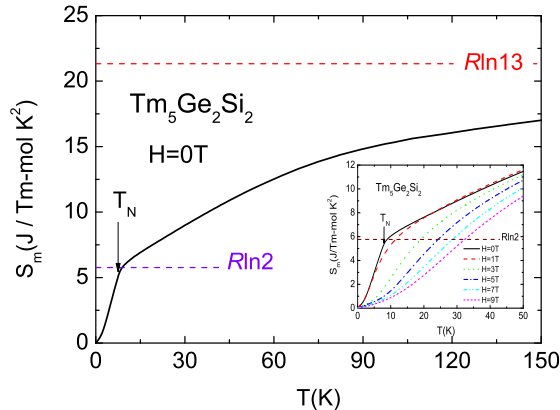


FIG. 10: (color online). Temperature dependence of the magnetic contribution ( $S_m$ ) to the entropy of  $\text{Tm}_5\text{Si}_2\text{Ge}_2$  single crystal at  $H=0$  T.  $R\ln 13$  and  $R\ln 2$  are the full entropies of  $\text{Tm}^{+3}$  and the entropy of a doublet ground state, respectively. The inset shows the entropy under magnetic fields.

fective magnetic moment using the following equation:  $p_{eff} = [\alpha \cdot p_{eff1}^2 + (1-\alpha) \cdot p_{eff2}^2]^{1/2}$ , where  $\alpha$  is the fraction of  $\text{Tm}^{3+}$  ions. Solving with respect to  $\alpha$ , the fraction of  $\text{Tm}^{3+}$  and  $\text{Tm}^{2+}$  ions in the unit cell is  $0.70 \pm 0.05$  and  $0.30 \pm 0.05$ , respectively. The fraction of each ion present can be estimated from the magnetization in the magnetically ordered state using the following equation:  $M = [\alpha \cdot M_{3+} + (1-\alpha) \cdot M_{2+}]$ . Solving with respect to  $\alpha$ , the fraction of  $\text{Tm}^{3+}$  and  $\text{Tm}^{2+}$  ions in the unit cell is  $0.70 \pm 0.03$  and  $0.30 \pm 0.03$ , respectively. The value of  $\alpha$  obtained from the saturating magnetic moment is equal to that obtained from the above mentioned effective magnetic moment. However, the mixed valent state differs from the result of the change in lattice constants.

In order to confirm the mixed valent state in more detail, the Tm 4d and 4p XPS spectra of  $\text{Tm}_5\text{Si}_2\text{Ge}_2$  was measured, as shown in Fig. 11. The XPS spectra of TmS and TmTe at the same core levels are also plotted as a reference for the  $\text{Tm}^{3+}$  and  $\text{Tm}^{2+}$  spectra, respectively. The Tm 4d and 4p XPS spectra of TmS have shoulders at the binding energies of 172 and 325 eV, respectively, which originate from the  $\text{Tm}^{2+}$  state appearing in the XPS spectra of TmTe. These spectral features are consistent with the mixed valent nature of TmS. [44] In  $\text{Tm}_5\text{Si}_2\text{Ge}_2$ , since the  $\text{Tm}^{2+}4d$  peaks do not appear in the both Tm 4d and 4p XPS spectra, the mean valence is almost trivalent compared to TmS. The Tm 4d and 4p XPS spectra of  $\text{Tm}_5\text{Si}_2\text{Ge}_2$  can be fitted by a linear combination of the XPS spectra of TmS and TmTe using the following function:  $I_{\text{Tm}_5\text{Si}_2\text{Ge}_2}(E) = \alpha \cdot I_{\text{TmS}}(E) + (1-\alpha) \cdot I_{\text{TmTe}}(E)$ . Here  $I_{\text{sample}}(E)$  indicates the XPS spectrum and  $\alpha$ , which is the fraction of TmS, becomes  $1.1 \pm 0.1$ . Since the mean valences of Tm ions in TmS and TmTe are 2.8 and 2.0, respectively, [43] the mean valence of  $\text{Tm}_5\text{Si}_2\text{Ge}_2$ ,  $z$ , can be estimated to be approximately  $2.9 \pm 0.1$  using the func-

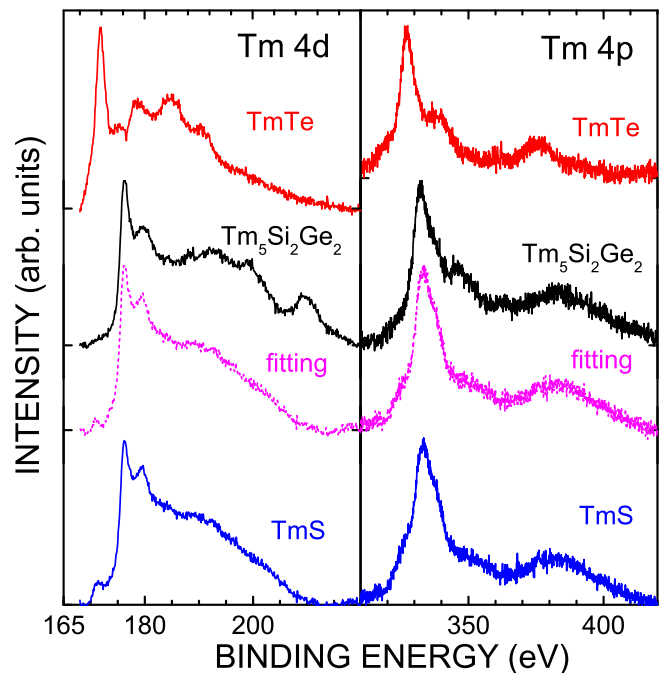


FIG. 11: (Color online) Tm 4d and 4p XPS spectra of  $\text{Tm}_5\text{Si}_2\text{Ge}_2$  and the reference materials, TmS and TmTe measured at  $T = 20$  K. The fitting results using the linear combination of  $1.1 \cdot I_{\text{TmS}}(E) - 0.1 \cdot I_{\text{TmTe}}(E)$  are also plotted.

tion  $z = 0.8 \cdot \alpha + 2.0$ . Therefore, the mean valence of Tm ions in  $\text{Tm}_5\text{Si}_2\text{Ge}_2$  evaluated from the XPS spectra was almost trivalent, which is consistent with the change in unit cell volume. The change in the lattice constants and XPS are more powerful than the magnetic susceptibility and magnetization because the formers are the results observed directly from a mixed valence. In this context, the reduced magnetic moment of Tm ions in  $\text{Tm}_5\text{Si}_2\text{Ge}_2$  is not due to the mixed valent state.

Spin frustration is often observed in triangular, Kagome and pyrochlore crystal structures.  $\text{Tm}_5\text{Si}_2\text{Ge}_2$  does not contain these structures, which excludes the spin frustration.

On the other hand, the phenomenon, in which conduction electrons strongly couple with f-electron spin in the opposite direction by a c-f interaction is known as the Kondo effect. The Kondo effect often causes a decrease in magnetic moment and the magnetic entropy. To confirm the correlation between these phenomena and the Kondo effect, this study measured the electrical resistivity of  $\text{Tm}_5\text{Si}_2\text{Ge}_2$  and  $\text{Lu}_5\text{Si}_2\text{Ge}_2$ , which does not contain 4f electrons and is a reference system for examining magnetic transport in  $\text{Tm}_5\text{Si}_2\text{Ge}_2$ . Fig. 12 shows their electrical resistivities.  $\text{Lu}_5\text{Si}_2\text{Ge}_2$  showed a normal metallic temperature dependence, while  $\text{Tm}_5\text{Si}_2\text{Ge}_2$  showed two anomalies below 10 K and approximately 200 K. To observe the anomalies in detail, the electrical resistivity of  $\text{Lu}_5\text{Si}_2\text{Ge}_2$  was subtracted from that of  $\text{Tm}_5\text{Si}_2\text{Ge}_2$ . The result is shown in Fig. 13. The anomalies revealed a log

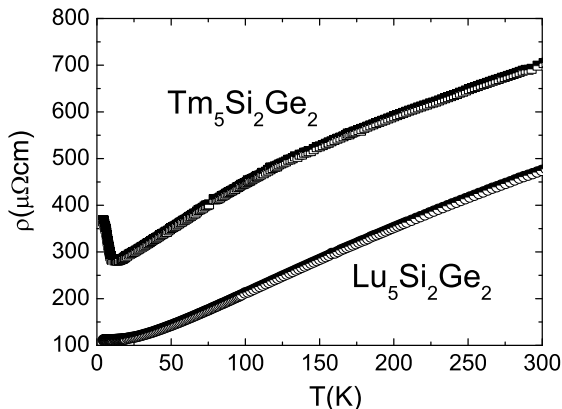


FIG. 12: (color online). Temperature dependence of the electrical resistivity of  $\text{Tm}_5\text{Si}_2\text{Ge}_2$  single crystal and  $\text{Lu}_5\text{Si}_2\text{Ge}_2$  poly crystal.

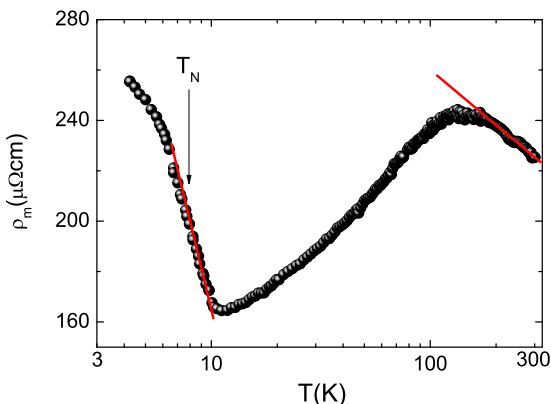


FIG. 13: (color online). Temperature dependence of the magnetic resistivity of  $\text{Tm}_5\text{Si}_2\text{Ge}_2$  subtracting the resistivity of  $\text{Lu}_5\text{Si}_2\text{Ge}_2$ .

$T$ -dependence. The  $\log T$ -behavior is a characteristic of the Kondo effect. The  $\log T$ -behavior observed in the low temperature regions begins from near  $T_N$ . In addition, the magnetic entropy of  $\text{Tm}_5\text{Si}_2\text{Ge}_2$  recovered to the full entropy of the ground doublet at  $T_N$ . This indicates that

the ground doublet state, which comes from the crystalline electric field (CEF) splitting for the Hund's rule ground state of  $J=6$ , is not affected by the Kondo effect, whereas the excited states near the ground state are affected by the Kondo effect. The  $\log T$ -behavior in high temperature regions is due to the Kondo effect for more excited CEF states. The Kondo temperature ( $T_K$ ) was estimated to be higher than 200 K according to the Kondo model. The high  $T_K$  interrupts the recovery of magnetic entropy at high temperatures, as mentioned above. The magnetic moments of the excited states screened by the Kondo effect should cause lower decrease in effective magnetic moment and magnetization. The Kondo effect is caused by the hybridization between conduction electrons and 4f electrons. the strength of hybridization depends on the overlap of their wavefunctions. When the excited crystal field orbits have a higher overlap with orbits of 5d conduction electron than the ground orbits, the Kondo effect due to the excited states dominates. This was well studied in Ce monopnictides [46].

#### IV. CONCLUSION

$\text{Tm}_5\text{Si}_2\text{Ge}_2$  crystallizes in an orthorhombic  $\text{Sm}_5\text{Ge}_4$ -type structure at 300 K. The long range antiferromagnetic order coupled along the  $b$  crystallographic axis is found below  $T_N=8.01$  K. Below about 5 K the antiferromagnetic magnetic moments coupled along the  $b$  crystallographic axis remain and the magnetic moments in the  $ac$  crystallographic plane are coupled ferromagnetically. The reduction of magnetic moment and magnetic entropy and  $-\log T$  dependence in electrical resistivity were observed in high temperature regions due to the Kondo effect on excited crystal field states. The competition between the Kondo effect and magnetic order plays an important role in  $\text{Tm}_5\text{Si}_2\text{Ge}_2$ .

#### Acknowledgments

This work was performed for the Nuclear R&D Programs funded by the Ministry of Science & Technology (MOST) of Korea.

- 
- [1] V.K. Pecharsky and K.A. Gschneidner, Jr., Phys. Rev. Lett. B **78**, 4494 (1997).
  - [2] V.K. Pecharsky and K.A. Gschneidner, Jr., Appl. Phys. Lett. **70**, 3299 (1997).
  - [3] L. Morellon, P.A. Algarabel, M.R. Ibarra, J. Blasco, B. Garcia-Landa, Z. Arnold, and F. Albertini, Phys. Rev. B **58**, R14 721 (1998).
  - [4] W. Choe, V.K. Pecharsky, A.O. Pecharsky, K.A. Gschneidner, Jr., V.G. Young, Jr., and G.J. Miller, Phys. Rev. Lett. **84**, 4617 (2000).
  - [5] E.M. Levin, V.K. Pecharsky, and K.A. Gschneidner, Jr., Phys. Rev. B **60**, 7993 (1999).
  - [6] L. Tan, A. Kreyssig, J. W. Kim, A. I. Goldman, R. J. McQueeney, D. Wermeille, B. Sieve, T. A. Lograsso, D. L. Schlagel, S. L. Budko, V. K. Pecharsky, and K. A. Gschneidner, Jr., Phys. Rev. B **71**, 214408 (2005).
  - [7] J. M. Cadogan, D. H. Ryan, Z. Altounian, H. B. Wang, and I. P. Swainson, J. Phys.: Condens. Matter **14**, 7191 (2002).
  - [8] G. H. Rao, Q. Huang, H. F. Yang, D. L. Ho, J. W. Lynn,

- and J. K. Liang, Phys. Rev. B **69**, 094430 (2004).
- [9] C. Ritter, L. Morellon, P. A. Algarabel, C. Magen, and M. R. Ibarra, Phys. Rev. B **65**, 094405 (2002).
- [10] L. Morellon, C. Ritter, C. Magen, P. A. Algarabel, and M. R. Ibarra, Phys. Rev. B **68**, 024417 (2003).
- [11] C. Magen, C. Ritter, L. Morellon, P. A. Algarabel, and M. R. Ibarra, J. Phys.: Condens. Matter **16**, 7427 (2004).
- [12] J. M. Cadogan, D. H. Ryan, Z. Altounian, X. Liu, and I. P. Swainson, J. Appl. Phys. **95**, 7076 (2004).
- [13] V. O. Garlea, J. L. Zarestky, C. Y. Jones, L. L. Lin, D. L. Schlagel, T. A. Lograsso, A. O. Tsokol, V. K. Pecharsky, K. A. Gschneidner, Jr., and C. Stassis, Phys. Rev. B **72**, 104431 (2005).
- [14] C. Ritter, C. Magen, L. Morellon, P. A. Algarabel, M. R. Ibarra, V. K. Pecharsky, A. O. Tsokol, and K. A. Gschneidner, Jr., J. Phys.: Condens. Matter **18**, 3937 (2006).
- [15] L. Morellon, C. Magen, P. A. Algarabel, M. R. Ibarra, and C. Ritter, Appl. Phys. Lett. **79**, 1318 (2001).
- [16] C. Ritter, L. Morellon, P. A. Algarabel, C. Magen, and M. R. Ibarra, Phys. Rev. B **65**, 094405 (2002).
- [17] L. Morellon, C. Ritter, C. Magen, P. A. Algarabel, and M. R. Ibarra, Phys. Rev. B **68**, 024417 (2003).
- [18] Kyunghan Ahn, A. O. Tsokol, Yu. Mozharivskiy, K. A. Gschneidner, Jr., and V. K. Pecharsky, Phys. Rev. B **72**, 054404 (2005).
- [19] A. O. Pecharsky, K. A. Gschneidner, Jr., V. K. Pecharsky, D. L. Schlagel, and T. A. Lograsso, Phys. Rev. B **70**, 144419 (2004).
- [20] J. M. Cadogan, D. H. Ryan, Z. Altounian, X. Liu, and I. P. Swainson, J. Appl. Phys. **95**, 7076 (2004).
- [21] A. O. Pecharsky, V. K. Pecharsky, and K. A. Gschneidner, Jr., J. Alloys Compd. **379**, 127 (2004).
- [22] H. F. Yang, G. H. Rao, W. G. Chu, G. Y. Liu, Z. W. Ouyang, and J. K. Liang, J. Alloys Compd. **334**, 131 (2002).
- [23] H. F. Yang, G. H. Rao, G. Y. Liu, Z. W. Ouyang, W. F. Liu, X. M. Feng, W. G. Chu, and J. K. Liang, J. Alloys Compd. **361**, 113 (2003).
- [24] H. F. Yang, G. H. Rao, W. G. Chu, G. Y. Liu, Z. W. Ouyang, and J. K. Liang, J. Alloys Compd. **339**, 189 (2002).
- [25] H. F. Yang, G. H. Rao, G. Y. Liu, Z. W. Ouyang, W. F. Liu, X. M. Feng, W. G. Chu, and J. K. Liang, J. Magn. Mater. **263**, 146 (2003).
- [26] H. F. Yang, G. H. Rao, G. Y. Liu, Z. W. Ouyang, W. F. Liu, X. M. Feng, W. G. Chu, and J. K. Liang, J. Alloys Compd. **346**, 190 (2002).
- [27] C. Magen, L. Morellon, P. A. Algarabel, M. R. Ibarra, C. Ritter, A. O. Pecharsky, K. A. Gschneidner, Jr., and V. K. Pecharsky, Phys. Rev. B **70**, 224429 (2004).
- [28] L. Morellon, Z. Arnold, C. Magen, C. Ritter, O. Prokhnenko, Y. Skorokhod, P. A. Algarabel, M. R. Ibarra, and J. Kamarad, Phys. Rev. Lett. **93**, 137201 (2004).
- [29] V. V. Ivtchenko, V. K. Pecharsky, and K. A. Gschneidner, Jr., Adv. Cryog. Eng. **46A**, 405 (2000).
- [30] K. A. Gschneidner, Jr., V. K. Pecharsky, A. O. Pecharsky, V. V. Ivtchenko, and E. M. Levin, J. Alloys Compd. **303**, 214 (2000).
- [31] G. S. Smith, Q. Johnson, and A. G. Tharp, Acta Crystallogr. **22**, 269 (1967).
- [32] G. S. Smith, A. G. Tharp, and Q. Johnson, Acta Crystallogr. **22**, 940 (1967).
- [33] S. Chikazumi, Physics of Ferromagnetism, 2nd ed. (Oxford Science, New York, 1997), 655 pp.
- [34] K. Held, M. Ulmke, N. Blumer, and D. Vollhardt, Phys. Rev. B **56**, 14469 (1997).
- [35] E. M. Levin, K. A. Gschneidner, Jr., T. A. Lograsso, D. L. Schlagel, and V. K. Pecharsky, Phys. Rev. B **69**, 144428 (2004).
- [36] Niraj K. Singh, S. Agarwal, K. G. Suresh, R. Nirmala, A. K. Nigam, and S. K. Malik, Phys. Rev. B **72**, 014452 (2005).
- [37] Niraj K. Singh, K. G. Suresh, R. Nirmala, A. K. Nigam, and S. K. Malik, J. Appl. Phys. **101**, 093904 (2007).
- [38] J. L. Wang, C. Marquina, M. R. Ibarra, and G. H. Wu, Phys. Rev. B **73**, 094436 (2006).
- [39] R. Nirmala, A. V. Morozkin, and S. K. Malik, Phys. Rev. B **75**, 094419 (2007).
- [40] J. A. Blanco, D. Gignoux, D. Schmitt, Phys. Rev. B **43**, 13145 (1991).
- [41] M. Bouvier, P. Lethuillier, D. Schmitt, Phys. Rev. B **43**, 13137 (1991).
- [42] R. Mallik, E. V. Sampathkumaran, Phys. Rev. B **58**, 9178 (1998).
- [43] K. G. Nath, Y. Ufukutepe, S. Kimura, Y. Haruyama, T. Kinoshita, T. Matsumura, T. Suzuki, H. Ogasawara and A. Kotani: J. Phys. Soc. Jpn. **72**, 1792 (2003).
- [44] E. Bucher, K. Andres, F. J. di Salvo, J. P. Maita, A. C. Gossard, A. S. Cooper and G. W. Hull Jr.: Phys. Rev. B **11**, 500 (1975).
- [45] J. Derr, G. Knebel, G. Lapertot, B. Salce, M.-A. Méasson and J. Flouquet, J. Phys.: Condens. Matter **18**, 2089 (2006).
- [46] H. Takahashi and T. Kasuya, J. Phys. C **18**, 2709 (1985).